



Variation of transverse and shear stiffness properties of wood in a tree

J. Xavier^{a,c,*}, S. Avril^b, F. Pierron^c, J. Morais^a

^a CITAB/UTAD, Engenharias I, Apartado 1013, 5001-801 Vila Real, Portugal

^b JS, ENSM-SE, 158 cours Fauriel, 42023 Saint-Etienne, France

^c LMFP, Arts et Métiers ParisTech, Rue St. Dominique BP 508, 51000 Châlons-en-Champagne, France

ARTICLE INFO

Article history:

Received 17 March 2009

Received in revised form 25 September 2009

Accepted 28 September 2009

Keywords:

A. Wood

B. Mechanical properties

D. Mechanical testing

ABSTRACT

In this work, the application of the unnotched Iosipescu test for the evaluation of the radial variability of longitudinal–radial stiffness parameters of maritime pine wood was investigated. Rectangular specimens with grain at 45° were tested using the Iosipescu fixture. For this configuration both the transverse (Q_{22}) and the shear (Q_{66}) stiffness parameters can be simultaneously identified by the virtual fields method. Displacement fields were measured by the grid method. The strain fields were reconstructed from the raw displacement fields using a polynomial approximation scheme. For the tested wood material, it was found that both parameters decrease from the centre to about the middle radius of the stem and increase afterwards to the outermost positions. Moreover, a relatively good correlation was obtained between the patterns of radial variability of Q_{22} and Q_{66} .

© 2009 Elsevier Ltd. All rights reserved.

1. Introduction

Wood is a biological material with a complex mechanical behaviour. At low levels of stress (below the elastic limit), short loading duration (a few minutes) and minor variations of moisture content and temperature (absence of hygro-thermal environment effects), wood is usually modelled as a linear elastic orthotropic material. Three directions of symmetry are locally defined: the longitudinal ($L, 1$), the radial ($R, 2$) and the tangential ($T, 3$) directions of the wood cells. Besides, at the macroscopic scale (10–200 mm), clear wood (free from structural features such as knots or gross grain deviation) can be analysed as a continuous and homogeneous material. In the longitudinal–radial (LR) plane, the constitutive linear elastic equations are completely determined by four stiffness or engineering parameters. Conventionally, these parameters are identified by carrying out several independent mechanical tests, from which a uniform or simple strain state is assumed in the gauge region (statically determined tests) [1].

During the tree growth the structure of the wood cells varies continuously namely because of environmental conditions and cambium age. As a consequence, the mechanical properties of wood can vary spatially within the stem of a tree. The quantification of these gradients is fundamental for assessing wood quality and, therefore, for the correct and the efficient utilisation of the wood material with regard to end-user needs and applications [2]. However, the studies addressing this subject have only consid-

ered the variations of mechanical properties of wood species (*i.e.*, elastic and strength properties) along the longitudinal (L) direction [3].

To our best knowledge, no information is available in the literature about the spatial variability of other elastic properties of wood species, such as the transverse (Q_{22}) and the shear (Q_{66}) stiffness properties. This lack of data may be justified by the fact that a great effort is required from an experimental point of view. Indeed, with standard tests, only one stiffness component will be obtained for each specimen type. This will not only lead to a great amount of test specimens but also to the fact that both stiffnesses will not be obtained on the same specimen. The relative variations of the different stiffness components within the same specimen and between specimens is potentially very interesting to study the effect of wood microstructure on properties and how both vary within the tree. Finally, tests to measure the transverse and shear stiffnesses in the LR plane are not easy. Only methods employing small test specimens will be suitable, such as the cube shear test based on Seichepine's test for composites [4]; but in this case load is introduced very close to the measurement area and St. Venant's assumption is not valid anymore, leading to potential experimental difficulties.

In view of all these experimental difficulties, the application of the unnotched Iosipescu test for assessing the radial variability of LR stiffness parameters of *Pinus pinaster* wood was investigated in this work. The procedure is based on the application of the virtual fields method (VFM) [5] to a small rectangular specimen loaded by the Iosipescu fixture. Wood specimens with grain at 45° were used because for this configuration both the Q_{22} and the Q_{66} stiffness parameters can be accurately identified by a single

* Corresponding author. Address: CITAB/UTAD, Engenharias I, Apartado 1013, 5001-801 Vila Real, Portugal. Tel.: +351 259 350 318; fax: +351 259 350 356.
E-mail address: jmcx@utad.pt (J. Xavier).

test [6], resulting in a significant reduction of the amount of specimens to be tested. Moreover, it will thus be possible to study the relative variations of both stiffness components with respect to the position in the tree.

2. Parameter identification from a statically undetermined test

2.1. Unnotched Iosipescu test

The mechanical test chosen in this work is the unnotched Iosipescu test (Fig. 1a) [5]. By removing the V-notches from the classical geometry of the Iosipescu specimen, it can be shown that a complex and heterogeneous strain field is generated across the central part of the specimen ($L \times W$, Fig. 1a), thanks to the shear/bending/compression stress distribution induced by the Iosipescu fixture. However, in order to identify a set of constitutive parameters, the contribution of each strain field components must be balanced out. In this test, this can be achieved by changing the length between the inner supports (L) and the grain (fibre) angle (θ) (Fig. 1a). The nominal dimensions of the specimen employed in this work were $80 \times 20 \times 5$ mm (Fig. 1b). Moreover, a free length $L = 34$ mm and an angle $\theta = 45^\circ$ were chosen, because in this configuration the identifiability of the transverse and the shear stiffness components is enhanced [6].

2.2. Full-field kinematic measurements

2.2.1. Grid method

The grid method is a white-light optical technique which measures in-plane full-field displacements by analysing the deformation of a grid, consisting of a periodic pattern of orthogonal bright and dark lines.

From a given image (light intensity field) of the grid, the phase, $\phi(x,y)$, of the 2π -periodic continuous function describing the grid pattern can be evaluated through a spatial phase-shifting method [7]. At least two images of the grid, taken before and after the application of an external load, are recorded and their corresponding phase maps evaluated. It can be shown that the difference of these phase fields is proportional to the displacement field, $u_\beta(x,y)$, by the following relationship:

$$u_\beta(x,y) = -\frac{p}{2\pi} \Delta \phi_\beta(x,y) \quad (1)$$

where $\beta = x$ or y , respectively, for the horizontal (vertical lines) or vertical (horizontal lines) components of the displacement.

2.2.2. Strain field reconstruction

The grid method measures the in-plane displacement field. Therefore, an additional numerical, denoising and differentiation procedure is required to calculate the corresponding strain field components needed in the material characterisation problem. This was achieved by fitting a 2D polynomial function to the raw (unfiltered) displacement data using a least-squares approximation scheme [6]. The strain field can then be straightforwardly deduced by differentiating the polynomial displacement fields. In the present application, a 7th-degree polynomial was found suitable for the least-squares regression scheme [6]. The reason why this works is that the spatial strain distribution is rather smooth (low spatial frequency contents).

2.3. Virtual fields method

The virtual fields method (VFM) is a suitable method for addressing the problem of parameter identification from full-field measurements [5]. It is based on the principle of virtual work (PVW), which can be written, in the case of plane stress approach and in absence of body forces, as:

$$\int_S \sigma_i \varepsilon_i^* dS = \frac{1}{t} \int_{S_f} T_\beta u_\beta^* dS \quad (i = 1, 2, 6 \text{ and } \beta = x, y) \quad (2)$$

where σ_i is the stress field, ε_i^* the virtual strain field, S the surface of interest of the plate, t the thickness of the plate, T_β the distribution of external tractions applied over S_f and u_β^* the virtual displacement field. Assuming a macroscopically homogenous material with an orthotropic linear elastic behaviour, the Eq. (2) can be rewritten as:

$$Q_{ij} \int_S \varepsilon_j \varepsilon_i^* dS = \frac{1}{t} \int_{S_f} T_\beta u_\beta^* dS \quad (3a)$$

with,

$$Q_{ij} = \begin{bmatrix} Q_{11} & Q_{12} & 0 \\ Q_{12} & Q_{22} & 0 \\ 0 & 0 & Q_{66} \end{bmatrix} = \begin{bmatrix} \frac{E_{11}}{1-\nu_{12}\nu_{21}} & \frac{-\nu_{21}E_{11}}{1-\nu_{12}\nu_{21}} & 0 \\ \frac{-\nu_{12}E_{22}}{1-\nu_{12}\nu_{21}} & \frac{E_{22}}{1-\nu_{12}\nu_{21}} & 0 \\ 0 & 0 & G_{12} \end{bmatrix} \quad (3b)$$

which involves the Q_{ij} stiffness parameters and the ε_j actual strain components over S , which must be measured by a suitable optical technique. In Eq. (3b), the symbols E , ν and G represent, respectively, the modulus of elasticity, Poisson's ratio and the shear modulus and the subscripts 1 and 2 denote the orthotropy axes.

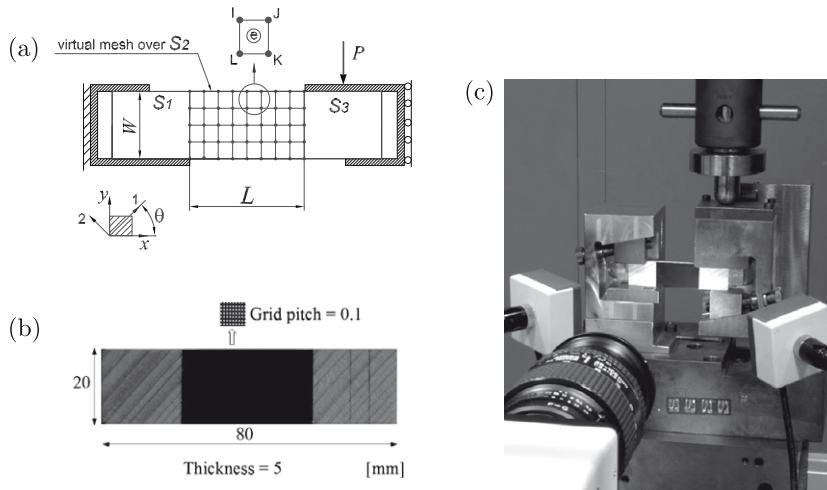


Fig. 1. (a) Schematic of the unnotched Iosipescu test (x - y and 1-2 are the specimen and material coordinate systems, respectively). (b) Specimen (configuration: $L = 34$ mm, $\theta = 0^\circ$). (c) Photomechanical set-up.

At this stage, Eq. (3a) is rewritten with as many independent kinematically admissible (i.e., continuous and differentiable) virtual fields as there are unknown Q_{ij} parameters. This procedure yields a linear system of equations, which must be solved in order to provide all the stiffness components.

Expressions for the direct identification of these parameters can be obtained through the so-called special virtual fields [5]. These virtual fields were expanded over a basis of piecewise functions with a mesh of 5×3 elements through the x and y directions. The solution was obtained through a constrained optimisation scheme which minimises the sensitivity of the VFM to noisy data (maximum likelihood solution). The details of this procedure can be found in [6].

3. Experimental work

3.1. Material and specimens

The wood material was manufactured from a single *P. pinaster* tree, aged of about 64 years (geographic origin: district of Viseu, Portugal). The tree was cut into several logs with a nominal length of 2.5 m, which were then converted into quartersawn and plainsawn boards. The boards were then dried in a kiln during several weeks in order to reach a moisture content of 12%.

The specimens were sampled from central boards (containing the pith) at two vertical locations within the stem, as schematised in Fig. 2. A first set was cut from the first log (Log 1) – vertical location 1 (l_1) – whereas the second one was manufactured from the third log (Log 3) – vertical location 2 (l_2). The specimens at location 1 were cut up from breast height (1.5 m above ground level) and the two vertical locations were separated by a distance of approximately 4 m. In order to evaluate the radial distribution of stiffness parameters at both vertical locations, rectangular specimens with nominal dimensions of $80 \times 20 \times 5$ mm were cut along the radial direction, from the pith to the outer part, and at an angle of 45° as shown in Fig. 2b. Due to some eccentricity and taper shape of the stem, the specimens were cut at four (r_1, r_2, r_3 and r_4) and three (r_1, r_2 and r_3) radial positions at the first (l_1) and second (l_2) vertical locations, respectively (Fig. 2). The radial positions were measured

and referenced from the pith and with regard to the geometrical centre of the specimens. At vertical location 1, radial positions r_1, r_2, r_3 and r_4 corresponded to about the 13th (29% of the radius), 19th (46% of the radius), 29th (64% of the radius) and 43th (81% of the radius) growth ring; whilst at vertical location 2, the radial positions r_1, r_2 and r_3 were at the 7th (30% of the radius), 16th (54% of the radius) and 30th (76% of the radius) growth ring. It is worth noticing that the region of interest of the specimens covers radially distinct annual growth rings (Fig. 2): at location 1, the regions of interest at r_1, r_2, r_3 and r_4 encloses, respectively, the 9–16th, 16–26th, 26–35th and 35–55th growth rings; whilst, at location 2, the regions of interest at r_1, r_2, r_3 contains, respectively, the 5–10th, 11–22th and 23–39th growth rings. The number of sampling points along the radius of the stem (four and three for locations 1 and 2, respectively, Fig. 2) is of the same order of other works addressing the radial variability of mechanical properties [3]. For repeatability quantification, at location 1, nine specimens per radial position were machined, i.e., a total of 36 specimens; whereas, at location 2, eight specimens per radial position were prepared, i.e., a total of 24 specimens. This was possible thanks to the 1.2 m length of the two boards. The authors are aware that this total number of specimens coming from a single tree is not enough for a representative study on the radial variation of the elastic properties of wood. Nevertheless, this is beyond the scope of this work, addressing the application of the unnotched Iosipescu test for assessing the radial variation of both the transverse and the shear stiffness parameters.

The mechanical tests were carried out at a room temperature of $23.2 \pm 1.2^\circ\text{C}$ and at a relative humidity of $42.7 \pm 4.9\%$. The oven-dry density (defined as the oven-dry weight to green volume ratio) of the specimens was found between 0.614 and 0.692 g cm^{-3} . The specimens were dried after testing and their moisture content estimated to $10.3 \pm 0.5\%$. Since the region of interest, over which the displacement field is measured, is confined to the centre of the specimen (Fig. 1a), X-ray microdensitometry measurements were also performed in order to estimate an average density by only taking into account the set of growth rings covering this region. These measurements were performed following the procedure described in Lousada [8]. Samples with nominal dimensions of $3(L) \times 5(T)$

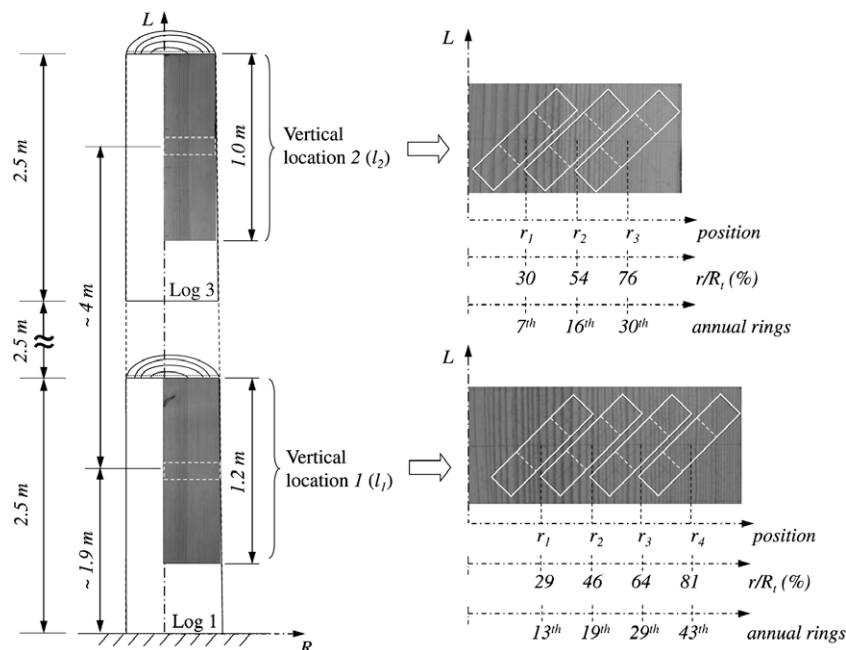


Fig. 2. Schematic representation of the specimens sampling within the stem.

and length equal to the local radius of the central boards were cut at both vertical locations 1 and 2. Measurement of density were performed with a spatial resolution of 0.1 mm.

3.2. Grid transfer

The pitch of the grid (p) was selected according to the size of the region of interest ($34(L) \times 20(W)$ mm²), the characteristics of the CCD sensor (pixel resolution of $1376(H) \times 1040(V)$; unit cell size of 6.45 μ m) and the number of pixels chosen for sampling one period ($N = 4$ pixels/period). Accordingly, a period (p) of 100 μ m was chosen, corresponding to a spatial frequency of 10 lines mm⁻¹. The grid was transferred to the surface of interest of the specimen according to the procedure described in [6]. In short, it consists in printing a grating pattern onto a photographic film (Ferrania photographic film Al PO-50®), and then transferring its printed coating to the specimen using a white epoxy resin (Epotechny E504®) (Fig. 1b).

3.3. Photomechanical set-up

In the photomechanical set-up (Fig. 1c), a 12 bit PCO SenSicam CCD Camera connected to a Nikon AF Micro-Nikkor 60 mm f-2.8D lens was used for image grabbing. The camera-lens system was mounted on a tripod and positioned in front of the specimen, with special care on the alignment of the sensor and grid planes (monovision system). The aperture of the lens ($f/8$), the exposure time ($1/8 = 0.125$ s), along with the working distance (i.e., the distance between the object and the front of the camera: $WD \approx 300$ mm) and light source intensity (LED Spotlight) were carefully selected in order to achieve a grid image of good quality. This means an image of the grid with enough contrast and a magnification setting leading to approximately four pixels per period (i.e., $m = 6.45 \mu\text{m}/25 \mu\text{m} = 0.258$). Images were recorded during the tests with an acquisition frequency of 2 Hz. It was also checked using a dial gauge that out-of-plane displacements were small enough not to cause significant parasitic strains arising from the change in magnification.

The spatial resolution of the grid method (i.e., the smallest distance separating two independent measurements) is practically equal to the period of the grid, i.e., 0.1 mm (gauge area of 34×20 mm²). The resolution (i.e., the smallest value that can be detected or measured) associated with the measurements was globally evaluated by the standard deviation of the residual map resulting from the difference of two phase fields of the same undeformed state of the grid/specimen. In our experiments, the phase resolution σ_θ was found to be about $3.05 \pm 0.5^\circ$. The displacement resolution (σ_u) was determined afterwards in the range of $1.20 \pm 0.2 \mu\text{m}$, according to $\sigma_u = \sigma_{\Delta\theta}/S$, where $S = 2\pi/p = 62.9 \text{ rad mm}^{-1}$. It may be worth mentioning that the scatter of the resolution obtained here was strongly related to the quality of the grid transfer achieved in each specimen. The strain resolution can be estimated from the noisy displacement maps (determined from images corresponding to the same mechanical field). A local differentiation approach, consisting in fitting a plane over a kernel of $P \times P$ pixels and determining the partial derivatives as its slopes through the x and y directions, will give an average strain resolution of about 1×10^{-4} , based on a 10 macro-pixels (spatial resolution of about 1.0 mm). This is of the same order of magnitude of other non-interferometric methods such as digital image correlation [9]. In this work, however, a global polynomial scheme (§2.2.2) was used. By applying this approach directly to the noisy displacement fields, strain fields characterised by a standard deviation (resolution) of 3×10^{-5} were typically obtained. This level of resolution is enough for measuring elastic strains.

The tests were carried out using an Instron 5582 universal testing machine and the a Iosipescu fixture. The load was measured by

a 5 kN load cell, with a controlled cross-head displacement rate of 1 mm min^{-1} .

4. Results and discussion

4.1. Radial variation of transverse and shear stiffnesses

As expected from the experimental validation reported in [6], the results for Q_{11} and Q_{12} (Eq. 3b) were too scattered and consequently no exploitable variability patterns could be clearly determined for these properties. This is justified by the fact that, for this specimen configuration, the ε_2 and the ε_6 components of the strain field are actually predominant. Therefore, only the results for Q_{22} and Q_{66} are exploitable and reported thereafter.

4.1.1. Transverse stiffness

The values of the transverse stiffness identified along the four radial positions at vertical location 1 ($Q_{22}(l_1, r_i)$; $i = 1, 2, 3, 4$), are reported and summarised in Fig. 3a.1 and Table 1. In terms of mean values, the Q_{22} stiffness decreases between the radial positions r_1 and r_2 and a progressive increase is observed up to r_4 . These values may be compared to each other using the t -test for equality of means of two samples (same variance) at a 95% confidence level. Accordingly, $Q_{22}(l_1, r_2)$ represents a different mean value when compared to the values at the other radial positions (r_1, r_3, r_4). Besides, $Q_{22}(l_1, r_1)$ represent statistically the same mean value as $Q_{22}(l_1, r_3)$ and $Q_{22}(l_1, r_4)$. The coefficients of variation (C.V.) associated to the Q_{22} mean values (Table 1) were in the same order of magnitude as the ones usually reported due to the inherent material variability when it comes to processing experimental results [10] (the scatter associated to other stiffness results, reported in Tables 1 and 2, are also in this acceptable order of magnitude).

The transverse stiffness values obtained radially at the upper vertical location 2 ($Q_{22}(l_2, r_i)$; $i = 1, 2, 3$) are presented in Fig. 3a.2 and Table 2. As it can be seen, Q_{22} decreases between r_1 and r_2 by 62% and increases afterwards from r_2 to r_3 by 72%. The $Q_{22}(l_2, r_2)$ clearly represents a different mean value with regard to both $Q_{22}(l_2, r_1)$ and $Q_{22}(l_2, r_3)$, which have been confirmed equal means.

4.1.2. Shear stiffness

The values of shear stiffness identified at vertical location 1 as a function of the radial positions ($Q_{66}(l_1, r_i)$; $i = 1, 2, 3, 4$) are reported in Fig. 3(b.1) and Table 1. Qualitatively, the pattern of spatial variation along the radial direction is the same as the one observed for Q_{22} (Fig. 3a.1), although with a lower contrast. The mean value of Q_{66} at the different radial positions were compared by the t -test of equality of means at a 95% confidence level. All values were found to represent the same mean, except for $Q_{66}(l_1, r_2)$. This confirmed a decrease of Q_{66} at around 46% of the radius of the stem. More stable properties were obtained at the outermost positions r_3 and r_4 , with a difference of only 4%.

Fig. 3(b.2) and Table 2 report the shear stiffnesses identified radially at vertical location 2 ($Q_{66}(l_2, r_i)$; $i = 1, 2, 3$). The same general trend as the one observed for Q_{22} at the same vertical location (Fig. 3a.2) was observed for the radial distribution of Q_{66} , although again with a lower spatial variability. It was confirmed by the t -test of equality of means that $Q_{66}(l_2, r_2)$ is a different mean when compared to both $Q_{66}(l_2, r_1)$ and $Q_{66}(l_2, r_3)$, which, in turn, represent the same mean value.

4.2. Influence of the longitudinal location on the stiffnesses

From the radial distributions of the Q_{22} and Q_{66} stiffness parameters at both vertical locations 1 (Fig. 3.1) and 2 (Fig. 3.2) – sepa-

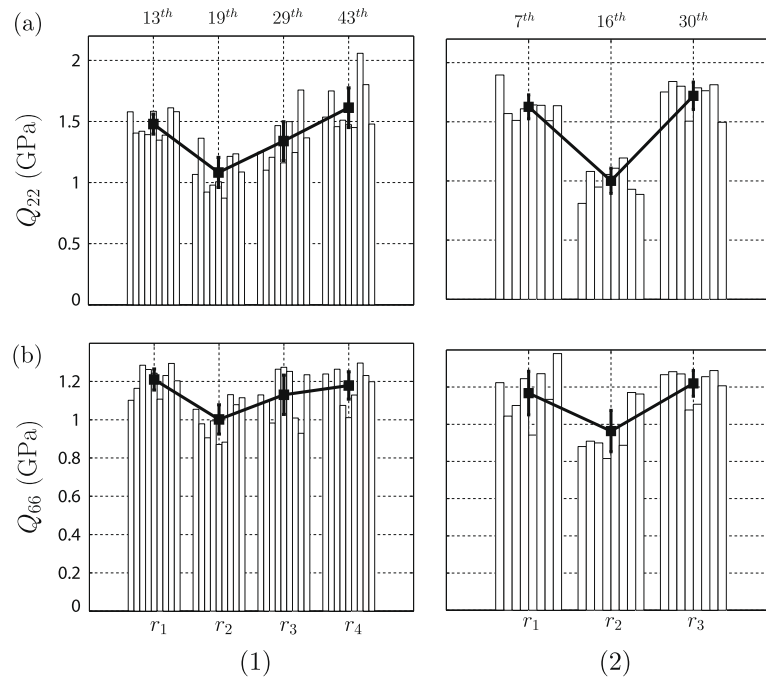


Fig. 3. (a) Q_{22} and (b) Q_{66} stiffness values determined along the radial direction (r_i) at vertical position 1 (1) and 2 (2). (□) Individual value, ■ mean value; ± standard deviation.)

Table 1

Q_{22} and Q_{66} stiffness values of *P. pinaster* wood identified across the radial positions r_i ($i = 1, 2, 3, 4$) at vertical location 1 (moisture content of about 10.4%).

	r_1 (13th)	r_2 (19th)	r_3 (29th)	r_4 (43th)
ρ^a				
Mean (g cm^{-3})	0.700	0.613	0.622	0.638
C.V. ^b (%)	0.94	3.96	1.37	5.44
Q_{22}				
Mean (GPa)	1.48	1.08	1.34	1.61
C.I. ^c	± 0.082	± 0.123	± 0.158	± 0.162
C.V. (%)	7.21	14.8	15.4	13.1
Q_{66}				
Mean (GPa)	1.21	1.00	1.13	1.18
C.I.	± 0.055	± 0.077	± 0.103	± 0.072
C.V. (%)	5.93	9.94	11.8	7.89

^a From X-ray microdensitometry measurements.

^b Coefficient of variation (%).

^c Confidence intervals at 95% confidence level (determined from the t -distribution after checking the normality by the Shapiro–Wilk test).

Table 2

Q_{22} and Q_{66} stiffness values of *P. pinaster* wood identified across the radial positions r_i ($i = 1, 2, 3$) at vertical location 2 (moisture content of about 10.3%).

	r_1 (7th)	r_2 (16th)	r_3 (30th)
ρ^a			
Mean (g cm^{-3})	0.678	0.622	0.642
C.V. ^b (%)	2.26	2.58	6.78
Q_{22}			
Mean (GPa)	1.63	1.00	1.72
C.I. ^c	± 0.102	± 0.107	± 0.115
C.V. (%)	7.47	12.8	8.02
Q_{66}			
Mean (GPa)	1.17	0.963	1.22
C.I.	± 0.117	± 0.112	± 0.069
C.V. (%)	12.0	13.9	6.79

^a Determined from the X-ray microdensitometry measurements.

^b Coefficient of variation (%)

^c Confidence intervals at 95% confidence level (determined from the t -distribution after checking the normality by the Shapiro–Wilk test).

rated by a distance of about 4 m (Fig. 2) – it can be concluded that no significant vertical variation exists between analogous radial positions. This is consistent with other studies [3], which have observed that, on the one hand, the longitudinal variation of wood properties is less significant than the radial one and, on the other hand, the longitudinal variation is only statistically significant among specimens taken at relatively high distances within the stem.

4.3. Relationship between transverse and shear stiffnesses

Several studies have addressed the relationships among wood properties in order to reduce the amount of experimental work necessary for wood characterisation [11] or to overcome experimental difficulties [12]. In this framework, the relationship between the radial distributions of Q_{22} and Q_{66} was investigated. This is reported in Fig. 4, where Q_{22} was plotted as a function of Q_{66} . Since no significant longitudinal variation was found among homologous radial positions, the data at the two vertical locations were collected together (Fig. 4). A regression scheme was applied to the data points to find out the degree of correlation. Linear and power functions have been employed. As it can be noticed, a relatively good relationship was found using both models with coefficient of correlations (R^2) of 0.895 ($Q_{22} = 2.58Q_{66} - 1.50$) and 0.894 ($Q_{22} = 1.09Q_{66}^{2.15}$), respectively.

4.4. Comparison of stiffnesses at the outermost radial position: mature wood

The Q_{22} and Q_{66} stiffness values determined from the set of specimens taken at the outermost radial position, at both vertical locations 1 (i.e., $Q_{22}(l_1, r_4)$ and $Q_{66}(l_1, r_4)$) and 2 (i.e., $Q_{22}(l_2, r_3)$ and $Q_{66}(l_2, r_3)$), can be directly compared with properties of *P. pinaster* wood reported in the literature [10] – it should be noticed that clear wood specimens for mechanical testing are generally taken at the outermost region of the stem, from where the properties of wood are expected to be more stable. Those properties were

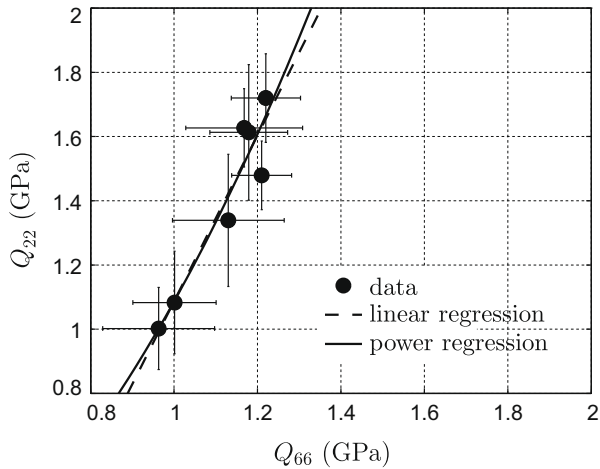


Fig. 4. Relationship between stiffness properties (linear regression: $Q_{22} = 2.58Q_{66} - 1.50$, $R^2 = 0.895$; one-term power regression: $Q_{22} = 1.09Q_{66}^{0.15}$, $R^2 = 0.894$). (● Mean value; \pm standard deviation.)

determined from statically determined mechanical tests, i.e., from tensile tests on specimens oriented along the radial direction and from the classical Iosipescu shear test on specimens oriented in the longitudinal–radial plane. This comparison is summarised in Fig. 5a and b, respectively, for Q_{22} and Q_{66} – it is worth noticing that the stiffness values in the reference were determined on specimens taken from a different tree of *P. pinaster* wood. Firstly, it can be concluded from the *t*-test for equality of means that the two pairs of properties identified at the two vertical locations, i.e. between $Q_{22}(l_1, r_4)$ and $Q_{22}(l_2, r_3)$ and between $Q_{66}(l_1, r_4)$ and $Q_{66}(l_2, r_3)$, represent the same mean value. Secondly, it can be noticed that lower values were systematically identified than the ones in the reference, although with differences, ranging from

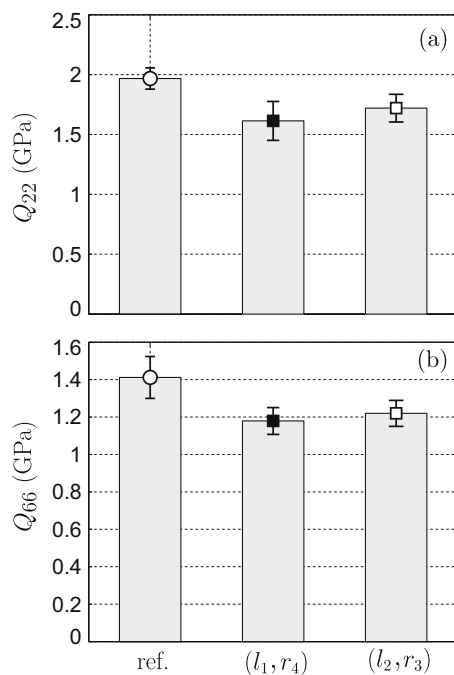


Fig. 5. (a) Q_{22} and (b) Q_{66} stiffness values (mean values and standard deviation), identified at location 1 (■) (i.e., vertical location l_1 and radial position r_4) and location 2 (□) (i.e., vertical location l_2 and radial position r_3), with regard to reference values [10] (○) (oven-dry densities (g cm^{-3}): $\rho_{\text{ref}} = 0.634$, $\rho(l_1, r_4) = 0.626$, $\rho(l_2, r_3) = 0.625$).

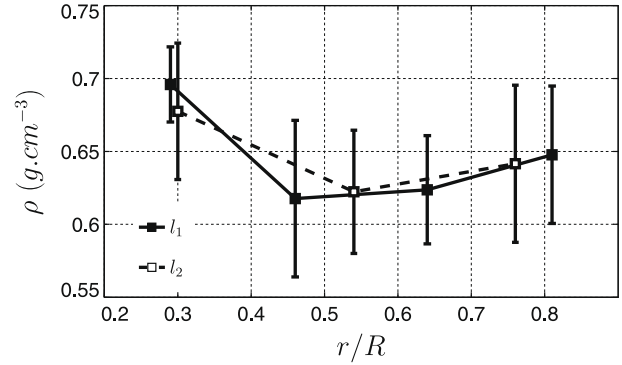


Fig. 6. Variation of the specimen density (ρ) (mean values and standard deviation) (determined from the X-ray microdensitometry measurements) along the radial direction at vertical locations 1 (■) and 2 (□).

13% to 18%, which can be assumed within the typical dispersion associated with the mechanical properties of wood. Besides, the oven-dry density of the specimens in the reference ($\rho_{\text{ref}} = 0.634 \text{ g cm}^{-3}$) were slightly greater than the one of the specimens tested in our study ($\rho(l_1, r_4) = 0.626 \text{ g cm}^{-3}$ and $\rho(l_2, r_3) = 0.625 \text{ g cm}^{-3}$); this is in agreement with the higher stiffness values.

4.5. On the structural variation of the specimens

The variation of the mean density of the specimens (determined from X-ray microdensitometry measurements) along the radius of the stem, at both vertical locations 1 and 2, is plotted in Fig. 6. As it can be seen, at vertical location 1 (■), the density is higher at the innermost position, decreasing around the centre of the stem and then slightly increasing at the outermost radial positions. At vertical location 2 (□), a similar pattern of density variation was also observed. The relative high dispersion (error bars) reflects the inherent variation of the local density of the growth rings within the specimens.

The relationship between the stiffnesses and the density of the tested specimens is analysed in Fig. 7. As can be concluded, the correlation of both the transverse ($R^2 = 35.4\%$) and shear ($R^2 = 46.6\%$) stiffnesses with regard to density is relatively weak. This means that the density by itself cannot explain the observed pattern of stiffness variation. Therefore, further investigations are needed in terms of spatial variation of the shape and the geometry of the cel-

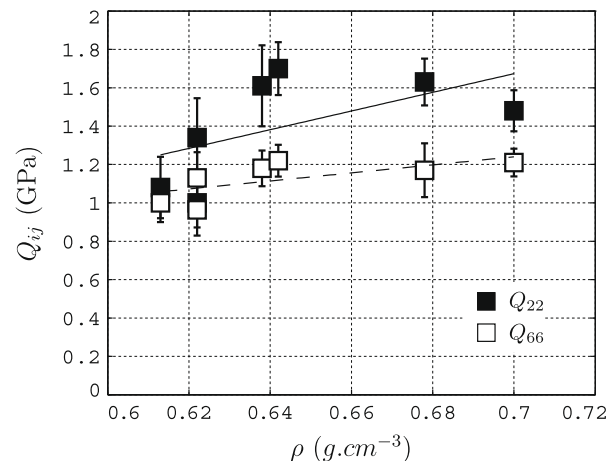
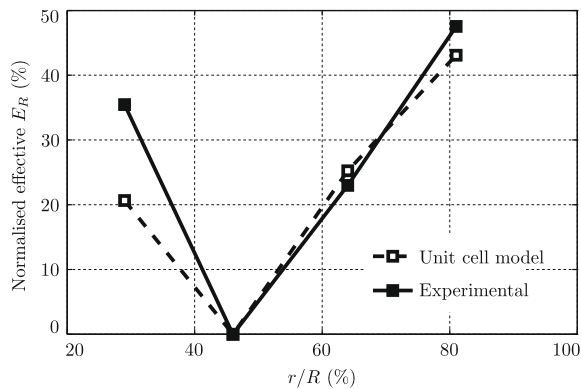


Fig. 7. Variation of Q_{22} (■) and Q_{66} (□) (mean values and standard deviation) with the specimens density (determined from the X-ray microdensitometry measurements) ($Q_{22} = 5.55\rho - 2.18$, $R^2 = 0.354$; $Q_{66} = 2.33\rho - 0.38$, $R^2 = 0.466$).

Table 3

Average parameters of the geometry of the wood cells along the radial direction, at vertical location 1.

Radial position	No. rings from pith	Earlywood			Latewood		
		Width (mm)	Cell wall thickness (μm)	Lumen width ^a (μm)	Width (mm)	Cell wall thickness (μm)	Lumen width (μm)
r_1	9–16	2.31	10.2	56.7	2.25	13.7	26.5
r_2	16–26	1.99	8.31	44.0	1.20	12.8	16.2
r_3	26–35	1.99	10.3	43.8	1.21	15.9	16.7
r_4	35–55	1.13	12.7	48.8	0.77	12.7	27.8

^a Along the radial direction.**Fig. 8.** Radial variation of the E_R modulus of elasticity as estimated by an unit cell model [14] with regard to the experimental data, at vertical location 1.

lular structure of wood. This is in the same spirit as other studies, for instance in which, besides the density, the microfibril angle has also been pointed as influencing the longitudinal stiffness [13].

Unit cell models have been proposed to estimate elastic properties of aggregates of wood cells, based on their shape and geometry [14]. These models are governed by several parameters of the geometry of the cells. Among them, two major parameters are the cell wall thickness and the radial width of the lumen. An attempt to measure the radial variation of these two geometrical quantities was done by processing images of wood cells taken from growth rings within the r_1 , r_2 , r_3 and r_4 positions at vertical location 1. These observations were carried out using an Olympus BX50 fluorescence microscope with amplification of $10\times$ (conversion factor of $0.46 \mu\text{m}/\text{pixel}$). The results are summarised in Table 3, where average values of the cell wall thickness and the lumen width, along the radial direction, have been evaluated for each earlywood and latewood constituents. In addition, the average width of the growth rings at those radial positions, measured by X-ray microdensitometry, has also been reported in Table 3. The width of the growth rings tends to decrease progressively along the radius of the stem, in which the width of the latewood layer represents in average 41.3% of the growth rings width. In terms of cell wall thickness, the smaller values were measured at position r_2 for both earlywood and latewood layers (Table 3) – this is in agreement with the lower density values measured at this position (Table 1). Besides, the cells with the smallest radial lumen width are located at the centre of the stem (radial positions r_2 and r_3) (Table 3). These geometrical parameters were used afterwards to estimate the radial variation of the E_2^1 engineering constant from the hexagonal unit cell model presented in [14] (in this model the tangential width at the edge (d_1) and centre (d_2) of the hexagonal cell were kept constant to 25 and $27 \mu\text{m}$, respectively). The effective values of E_2 were evaluated by the law of mixtures (series model) from the ear-

lywood (E_2^{EW}) and latewood (E_2^{LW}) properties (which were estimated from the cell wall thickness and lumen radial width of each cell type, Table 3) and relative percentage of each constituents within the growth rings. For the purpose of comparison, results predicted from the cellular model and experimental data were normalised with regard to the value at radial position r_2 (Fig. 8). This means that the model is only used to predict stiffness contrast and not absolute values (that depends on many unknown parameters). As it can be seen, a relatively good agreement was found in terms of pattern distribution and contrast variation of the stiffness along the radial position. The pattern obtained from the cellular model is mainly affected by the cell wall thickness – since the stiffness evolves with the cube of this parameter – which reaches its smallest value at radial position r_2 (Table 3).

5. Conclusions

In this study, the unnotched Iosipescu test was applied for investigating the radial variability, on the longitudinal($L,1$)–radial($R,2$) symmetrical plane, of both the transverse (Q_{22}) and the shear (Q_{66}) stiffness properties of *P. pinaster* wood in a tree.

Advantages of using this test method were the fact that relatively small specimens were used and that both the Q_{22} and Q_{66} stiffness properties could be simultaneously determined on a single configuration with grain at 45° . In order to assess the radial variation of both stiffnesses, rectangular specimens were sampled at distinct and successive (three/four) positions along the radius of the stem at two vertical locations. The displacement fields were measured experimentally by the grid method, over the central region of interest of the specimens. The strain fields were then reconstructed by fitting a 2D polynomial to the raw displacements by means of a global least-squares regression scheme. Finally, the strain fields, together with the load and the geometry data, were processed by the virtual fields method in order to extract the stiffness parameters activated in the mechanical response of the specimen.

It was found that both the Q_{22} and the Q_{66} parameters decreased from the innermost position to about the middle radius of the stem and increased afterwards to the outermost positions. Although, the radial variability of Q_{22} was higher than the one obtained for Q_{66} . Moreover, a good correlation was found between the patterns of radial distribution of Q_{22} and Q_{66} . Finally, by comparison of stiffness values at the outermost radial position with *P. pinaster* properties reported in the literature and determined from conventional mechanical tests, a good agreement was found in terms of both mean and dispersion values.

Structural features such as density and geometry of the wood cells were measured in order to figure out their influence on the observed pattern of stiffnesses variation. On the one hand, it was found that the radial distribution of the densities qualitatively follows the same pattern as the ones determined for the stiffnesses. However, for the tested specimens, a relatively weak correlation between stiffnesses and density was observed. On the other hand, from the values of transverse stiffness, evaluated from geometric

¹ Considering Eq. (3b) and the elastic properties of *P. pinaster* wood reported in [10], the following relationship can be obtained: $Q_{22} = 1.03E_2$.

parameters of the wood cells by considering an hexagonal unit cell model, it was also concluded a reduction of the stiffness values at the centre of the stem because, in this region, the wood cells have the smallest thickness on both earlywood and latewood layers. It was finally found that the model could give a fairly honest description of the evolution of the radial modulus, thus demonstrating the essential role of cell wall thickness, and confirming the quality of the experimental results obtained with the virtual fields method.

Acknowledgements

We would like to thank João Luís Pereira and Marcelo Oliveira for their help in the wood material preparation, José Luis Louzada for his help in the X-ray microdensitometry measurements and the Foundation for Science and Technology (FCT) for J. Xavier's Ph.D. scholarship.

References

- [1] Smith I, Landis E, Gong M. Fracture and fatigue in wood. John Wiley and Sons; 2003.
- [2] Tsehay A, Buchanan A, Walker J. Selecting trees for structural timber. Holz Roh Werkst 2000;58(3):162–7.
- [3] Machado J, Cruz H. Within stem variation of maritime pine timber mechanical properties. Holz Roh Werkst 2005;63(2):154–9.
- [4] Whitney J, Daniel IPRB. Experimental mechanics of fiber reinforced composite materials. Englewood Cliffs (NJ): Prentice Hall; 1984.
- [5] Grédiac M, Pierron F, Avril S, Toussaint E. The virtual fields method for extracting constitutive parameters from full-field measurements: a review. Strain 2006;42(4):233–53.
- [6] Xavier J, Avril S, Pierron F, Morais J. Novel experimental approach for longitudinal–radial stiffness characterisation of clear wood by a single test. Holzforschung 2007;61(5):573–81.
- [7] Surrel Y. Fringe analysis. In: Rastogi P, editor. Photomechanics (Topics in applied physics). Springer-Verlag; 1999. p. 57–104.
- [8] Lousada J. Variação fenotípica e genética em características estruturais na madeira de *Pinus pinaster* Ait., Ph.D. thesis, Universidade de Trás-os-Montes e Alto Douro, Vila Real, Portugal [in Portuguese]; 2000.
- [9] Hild F, Roux S. Digital image correlation: from displacement measurement to identification of elastic properties – a review. Strain 2006;42(2):69–80.
- [10] Xavier J, Garrido N, Oliveira J, Morais J, Camanho P, Pierron F. A comparison between the Iosipescu and off-axis shear test methods for the characterization of *Pinus pinaster* Ait. Compos Part A – Appl Sci 2004;35(7–8):827–40.
- [11] Bodig J, Goodman R. Prediction of elastic parameters for wood. Wood Sci 1973;5(4):249–64.
- [12] Liu J, Ross R. Relationship between radial compressive modulus of elasticity and shear modulus of wood. Wood Fiber Sci 2005;37(2):201–6.
- [13] Xu P, Donaldson L, Walker J, Evans R, Downes G. Effects of density and microfibril orientation on the vertical variation of low-stiffness wood in radiata pine butt logs. Holzforschung 2004;58(6):673–7.
- [14] Thuvander F, Jernkvist L, Gunnars J. Influence of repetitive stiffness variation on crack growth behaviour in wood. J Mater Sci 2000;35(24):6259–66.